

Global basic landform units derived from multi-source digital elevation models at 1 arc-second resolution

Xin Yang^{1,2,4†}, Sijin Li^{1,2,4†}, Junfei Ma^{1,2,4}, Yang Chen^{1,2,4}, Xingyu Zhou^{1,2,4}, Fayuan Li^{1,2,4}, Liyang Xiong^{1,2,4}, Chenghu Zhou³, Guoan Tang^{1,2,4*} & Michael E. Meadows^{5,6*}

[†] These authors contributed equally to this work.

^{*} Co-corresponding authors: Guoan Tang tanggaoan@njnu.edu.cn; Michael E Meadows michael.meadows@uct.ac.za

¹School of Geography, Nanjing Normal University, Nanjing, 210023, China

²Key Laboratory of Virtual Geographic Environment (Nanjing Normal University), Ministry of Education, Nanjing, 210023, China

³Institute of Geographical Information Science and Natural Resources, Chinese Academy of Science, Beijing, 100101, China

⁴Jiangsu Centre for Collaborative Innovation in Geographical Information Resource Development and Application, Nanjing 210023, China

⁵School of Geography and Ocean Sciences, Nanjing University, Nanjing 210023, China

⁶Department of Environmental & Geographical Science, University of Cape Town, Rondebosch 7701, South Africa

Abstract. Landforms are fundamental components of the Earth surface, providing the base on which surface processes operate. Understanding and classifying global landforms, which record the internal and external dynamics of the planet's evolution, constitutes a critical aspect of Earth system science. Advances in Earth observation technologies have enabled access to higher resolution data, for example remote sensing imagery and digital elevation models (DEMs). However, landform data with a resolution of approximately 1 arc-second (approximately 30 m) are lacking at the global scale, which limits the progress of geomorphologic studies at finer scales. Here, we propose a novel framework for global landform classification and release a unique dataset called Global Basic Landform Units (GBLU), which incorporates a comprehensive set of objects that constitute the range of landforms on Earth. Constructed from multiple 1 arc-second DEMs, GBLU ranks among the highest-resolution global geomorphology datasets to date. Its development integrates geomorphological ontologies and key derivatives to strike a balance between mitigating local noise and preserving valuable landform details. GBLU categorizes the Earth's landforms into three levels with 26 classes, yielding discrete vector units that record landform type and distribution. Comparative analyses with previous datasets reveal that GBLU enhances capture of landform details, enabling more precise depiction of geomorphological boundaries. This refinement facilitates the identification of novel spatial disparities in landform patterns, exemplified by marked contrasts between Asia and other continents, and highlights the distinct prominence of China in terms of landform diversity. Given that the fundamental data resolution of GBLU accords well with available remote sensing datasets, it is readily incorporated into analytical workflows, exploring the relationship between landforms, climate and land cover. The full data set is available on the Deep-time Digital Earth Geomorphology platform and Zenodo (Yang et al., 2024; <https://doi.org/10.5281/zenodo.13187969>).

1. Introduction

Approaches to geomorphology vary, and include research on, for example, genesis, processes, materials, hazard and risk, and chronology, but the essential basis of all of these studies is the *landform* (Evans, 2012), which can be regarded as the ‘final surface status’ resulting from the combined influence of various forces. The morphology of landforms and their associated evolutionary processes have long been a source of fascination, leading ultimately to the development of the formal science of geomorphology (MacMillan and Shary, 2009). Classifying and mapping the Earth’s surface into landform types according to morphological characteristics is a primary means of understanding surface patterns and processes on planet Earth (Evans, 2012; Xiong et al., 2022) and advancement in this field has potential benefits for the more efficient allocation of global resources to promote sustainable development (Dramis, 2009).

Traditional landform mapping primarily relies upon manual interpretation, the survey based on the field work, topographic maps and aerial photographs supported by field investigations (Drăguț and Blaschke, 2006; Hammond, 1954; Iwahashi et al., 2018; Pennock et al., 1987). However, a series of technological developments has facilitated the automation of landform classification in recent decades, largely dependent on topographic derivatives calculated from DEMs, such as slope, aspect, relief, curvature, roughness (Jasiewicz and Stepinski, 2013; Amatulli et al., 2018, 2020; Dyba and Jasiewicz, 2022; Snethlage et al., 2022). With the

development of earth observation systems and DEM refinement, several global landform datasets based on this framework have been proposed using various data sources and at different levels of spatial resolution (Florinsky, 2017; Iwahashi and Yamazaki, 2022). Using a decision tree algorithm and 1-km SRTM30 data, Iwahashi and Pike (2007) generated a global terrain classification gridded dataset containing 16 undefined topographic types determined by slope gradient, local convexity, and surface texture. Relying on elevation and the standard deviation of elevation, Drăguț and Eisank (2012) adopted an object-based method to automatically classify global landforms from SRTM data resampled to 1 km. Meanwhile, Iwahashi et al. (2018) improved their previous work and established 15 landform classes based on MERIT DEM. To further eliminate issues involved in detecting narrow valley bottom plains, metropolitan areas, and slight inclines in otherwise largely flat plains, Iwahashi and Yamazaki (2022) introduced the elevation above the nearest drainage line measure, and achieved landform classification based on a DEM at 90m resolution. However, as the authors stated, unsupervised classification-based methods to perform higher-resolution global landform classification require an international team with knowledge of geomorphological development in a variety of climatic and physiographic settings (Iwahashi and Yamazaki, 2022). In addition, at regional and/or global scales, several researchers have achieved automated landform classification following the Hammond procedure (Gallant et al., 2005; Karagulle et al., 2017; Martins et al., 2016). All these datasets have provided valuable resources to explore surface patterns, and also played important roles in supporting related disciplines such as hydrology, pedology, and ecology among others.

However, shortfalls remain in current landform classification research and require attention to the following points. Firstly, previous studies have adopted relatively coarse resolution DEMs, resulting in an inaccurate depiction of topographic information. Recent developments in Earth observation technology have concentrated on the deployment of digital elevation models (DEMs), which contain abundant geometric information about surface relief (Drăguț and Eisank, 2011), although the approach and methods of implementing landform classification have not kept pace with advances in DEM resolution and quality. Nevertheless, higher DEM data resolution can be regarded as a double-edged sword, in that it at once provides the opportunity for landform mapping at a finer scale while at the same time increasing the challenge of reducing the negative effect of the data noise and abrupt terrain variations (Jasiewicz and Stepinski, 2013) and maintaining the morphological integrity of the identified landforms. Secondly, at the global scale, diverse and complex environmental factors have increase the complexity landform morphology that pose substantial challenges to the generalizability of classification methods (Li et al., 2020). With increasing human impact on landforms, a re-evaluation of landform classification that takes advantage of an increasingly potent digital database and ongoing improvements in human understanding of landform evolution and processes seems opportune. Finally, landform information obtained from a particular metric is derived at a particular spatial scale, determined jointly by the DEM resolution and window size in the neighborhood analysis, giving rise to uncertainties in the landform classification results.

Therefore, the development of innovative classification approaches and systems based on high resolution DEMs remains a priority for research on global landforms. In this study, we conduct a classification and mapping of global landforms based on a DEM at 1 arc-second resolution. We focus on the classification of basic landforms that emphasizes morphological differences and,

in so doing, we present the practical expression of landform ontology at the global scale that offers valuable insights into the Earth's surface structure comprising the constellation of landform types and their boundaries. The objectives of this research are: (1) to construct a global classification system for landforms that integrates domain consideration of landform-related studies, (2) to design a novel framework for global basic landform classification, (3) to develop an automated classification and mapping model for global landforms, and (4) to make available a comprehensive global dataset of landform units.

2. Methodology

2.1 Hierarchical classification system and data

In aiming to provide a comprehensive classification of landforms at the global scale, our study encompasses all terrestrial regions worldwide, including islands and polar areas. Identifying landform objects and constructing a classification system is a preliminary and significant step in geomorphological and landform classification studies. It is crucial to recognize that landforms not only represent assemblages of quantitative characteristics but also convey the basic human understanding of nature (Smith and Mark, 2001). For example, the identification of what is acknowledged as a 'mountain' is as much a product of human perception as of its natural characteristics (Smith and Mark, 2003), thus emphasizing the importance of incorporating human understanding and domain application into landform classification and mapping. In this study, we focus here on the classification of basic landforms that emphasizes morphological differences that are not only perceptible to humans but also constitute vital components in the analysis of surface environments.

In taking into consideration the complexity of global landform characteristics, the classification criteria should satisfy the following requirements: (1) the determined classes should be globally applicable; (2) the setting of the landform types should conform with the current knowledge domain of geomorphology; and (3) specific criteria should be able to be interpreted and applied. The term "landform" is inherently scale- and context-dependent. In this study, we specifically emphasize force accumulation, mountain ecosystems, and microclimatic gradients before constructing the classification system. After comprehensive consideration of numerous classification systems, we propose a set of criteria for basic landform classification, primarily based on (Zhou et al., 2009). The new criteria integrate the typical rules of landform classification with indices proposed in this work, and are aimed at reflecting human knowledge in a quantitative way. We establish a hierarchical classification system comprising 3 levels and 23 classes (Table A1), thereby advancing a structured framework for understanding Earth's diverse landscapes. The first-level (L1) corresponds to the conventional concept of a complete landform entity, while the second level (L2) and third level (L3) provide progressively finer-scale morphological information. L1 types are defined as 'plain' and 'mountain', reflecting the most fundamental morphological characteristics of landforms. Plains and mountains are the most direct reflection of the combined effects of geomorphological processes and profoundly influence biological activities. This classification perspective aids researchers in conducting macro-scale studies. At L2, plain landforms retain their labels to guarantee completeness of the classification system, and are further divided into low-altitude, middle-altitude, high-altitude, and highest-altitude plains based on elevation. Mountains

are subdivided at L2 into hills and other mountains with varying degrees of relief. At L3, we provide a further detailed classification of hills and mountains based on elevation.

To attain global coverage, we utilize three DEM datasets (Table 1). These datasets are publicly available for access and have been widely used in geomorphological studies, ensuring their accuracy and validity. In this work, the ‘Forest and Buildings removed Copernicus DEM’ (FABDEM) (Hawker et al., 2022) is the primary data for latitudes 60°S-80°N. This dataset is the first bare-earth DEM dataset at a global scale at 1 arc-second (approximately 30-meter) resolution, developed using machine learning techniques from Copernicus DEM. By eliminating the bias resulting from building and vegetation heights, some terrain features, such as slope, aspect, and watersheds, can be estimated more accurately, which is of significant benefit in landform classification. Meanwhile, the Advanced Land Observing Satellite (ALOS) World 3D - 30 m (AW3D30) (Tadono et al., 2014) dataset is used to supply data for the area missing from FABDEM. In addition, to avoid the negative impact of ocean pixels on landform classification results, the OpenStreetMap (OSM) Land Polygon was utilized as a mask to eliminate the sea.

Table 1. Data sources and attributes

	FABDEM	AW3D30 V3.2	REMA
Spatial Coverage	60°S-80°N	82°S-82°N	56°S-88°S
Spatial Resolution	1 arc-second	1 arc-second	32 m
Vertical Accuracy	<4 m	4.4 m (RMSE)	4 m (RMSE)
Release Date	2021	2021	2022
Data link	https://data.bris.ac.uk/data/dataset/s5hqmjcdj8yo2ibzi9b4ew3sn	https://www.eorc.jaxa.jp/ALOS/jp/data/aw3d30/aw3d30_j.htm	https://www.pgc.umn.edu/data/rema/

2.2 Global landform classification method

In this study, we propose a new framework and provide the corresponding implementation workflow. The proposed method of global landform classification has a hierarchical structure, involving data pre-processing, identification of mountains and plains, calculation of the surface relief index (SRI), landform classification, and post-processing. Figure 1 illustrates the workflow. The following sections provide details that should allow users to reproduce our results. In this study, we built characteristic quantification and landform classification models based on tools in ArcGIS Pro. A detailed description of the step-by-step procedures follows below.

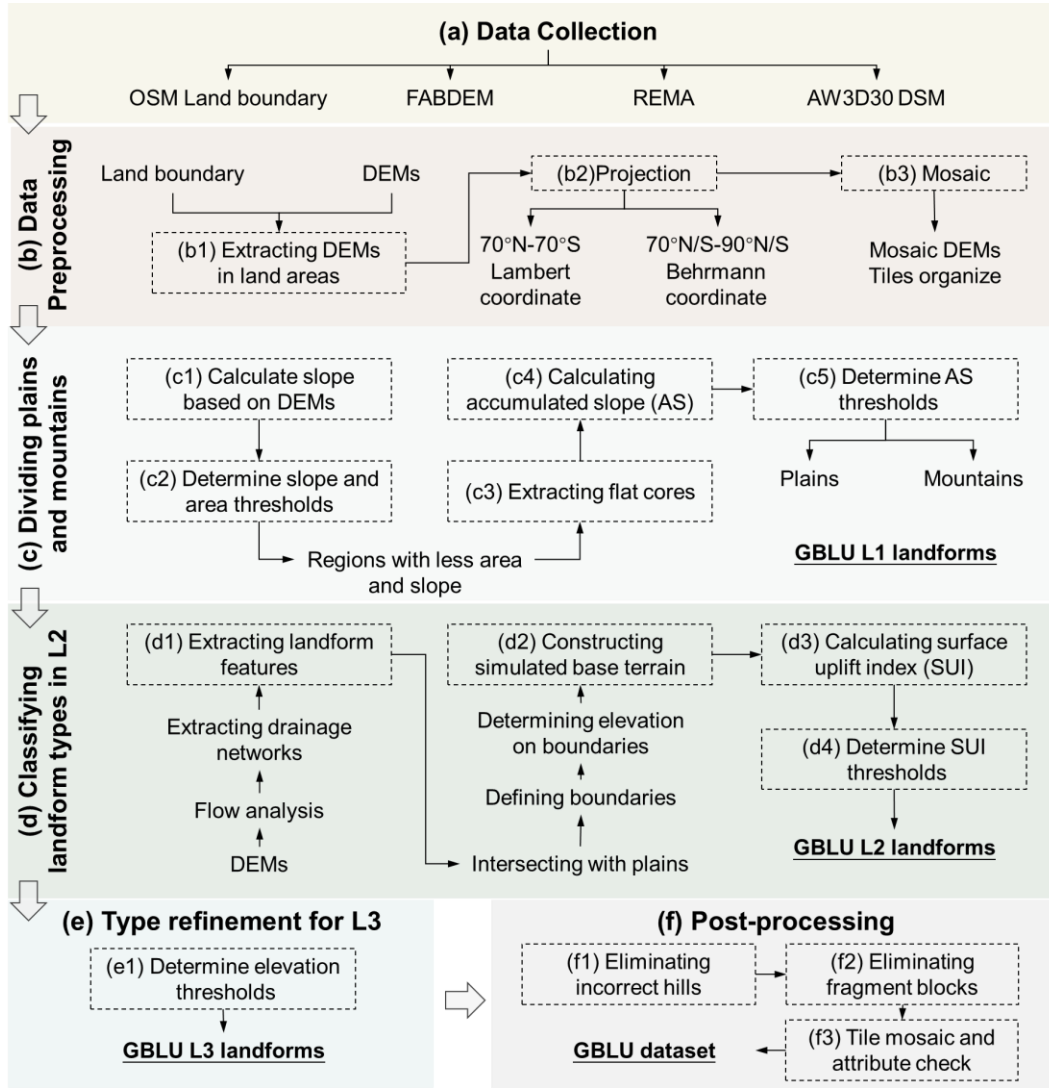


Figure 1. Workflow for global landform classification used in this study.

2.2.1 Data preprocessing

As shown in Figure 1b, data pre-processing focuses primarily on land area extraction and data merging. We use the OSM land polygon as the land mask to eliminate the marine pixels that negatively influence subsequent processes. To improve processing efficiency, the original DEM elements with size of 1×1 degree are mosaiced to tiles of 10×10 degrees. Meanwhile, due to the requirement of calculating landform derivatives, we determine the projection principles as follows: Tiles between 70° N/S are reprojected to the equal area Behrman projection, and the tiles polewards of 70° N/S to Lambert azimuthal equal-area. To mitigate border effects between the two projection zones, we have implemented an overlapping strategy in our processing. Specifically, we processed the DEMs in $11^\circ \times 11^\circ$ tiles, ensuring that the main $10^\circ \times 10^\circ$ area is used as the final output. This approach helps maintain consistency and minimizes distortions at the transition between projection zones. For consistency and ease of use, the final TIFF files have been reprojected into a single coordinate system (EPSG:3857)

2.2.2 Identifying plains and mountains

Identifying and distinguishing contrasting plains and mountains represents the initial step in basic landform classification and mapping. We have designed a practical framework based on landform ontology to classify plains and mountains. The plains can

be separated into core, transition and boundary, whereby the core represents areas with the most typical flat characteristics, i.e. very low relief. Transitions have plain cores but also contain sloping elements, i.e. areas that in part satisfy their classification as plain but also exhibit sloping characteristics not typical of plain. Misclassifications usually occur in transition areas due to their atypical characteristics. Meanwhile, the boundary represents the part of the plain area where the geomorphological semantics and labels change to the mountain.

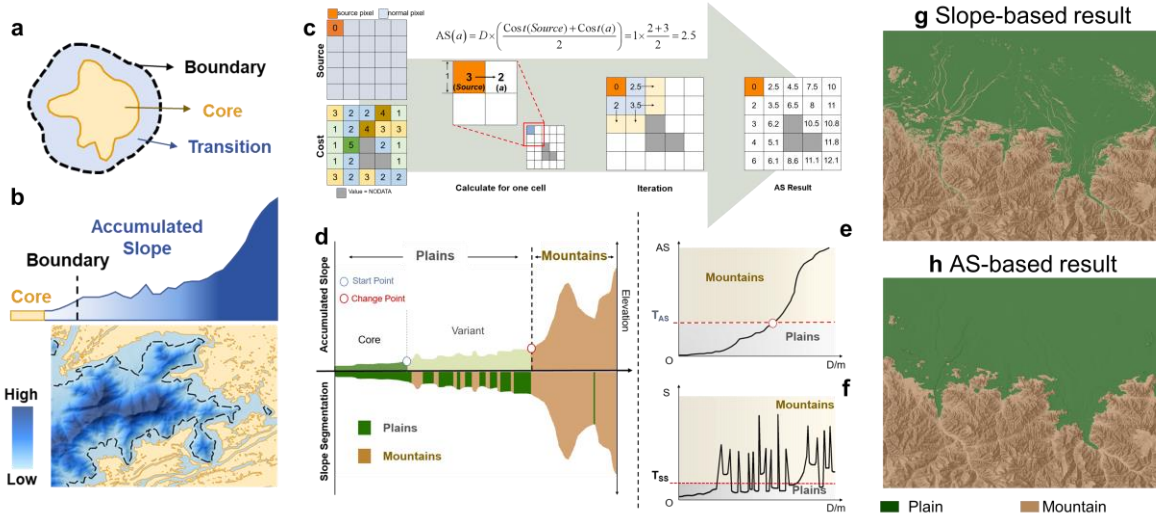


Figure 2. Illustration of calculation methods. **a** Conceptualization of plains. **b** calculation principle and results of accumulated slope (AS), respectively. **c** schematic diagram of the cost-distance algorithm. The cost refers to the slope in this process. **d** profile reflecting landform composition according to the proposed conceptual model of plains, segmented based on the slope; **e** calculated result of the AS and **f** calculated result of slope, where T_{AS} is the threshold of AS, and T_{SS} is the threshold of surface slope. For Figures 2c and d, areas smaller than the threshold are classified as plains (marked in green), while the remaining areas are classified as mountains (marked in brown). **g** and **h** comparison of the AS and slope indicators in the division of plains and mountains.

Firstly, we regard the areas with low slope angles as the plain cores. Here, the slope threshold (T_1) is recommended to be set as 1.5-3 degrees according to our global pre-assessment experiments. Areas where the slope angle lies below the threshold T_1 are classified as plain cores. A block must be greater than 0.1 km² to be classified as a core plain area. In landform classification, the core areas of each landform are typically distinct and can be accurately identified. However, there is significant ambiguity in the transitional zones and boundaries between different landform types. To address this issue, we propose reexamining landform classification from an ontological perspective. In information science, an ontology is a neutral and computationally tractable description of a given individual or category which can be accepted and reused by all information gatherers (Smith and Mark, 2003). In this study, based on the spatial information theory, we propose a conceptual description of landforms that enhances the generalization of landform and reduce the negative influence of vagueness. Considering that the characteristics of plains are more distinct and their definition is clearer, we will use plains as the foundation for expanding the landform ontology. As shown in Figure 2a, the conceptual model of plains includes three elements, viz. core, transition and boundary. The plain core represents areas with the most typical plain characteristics, i.e. very low relief. Transitions are areas with elements consistent with the plain cores but also contain non-standard slope characteristics. In other words, transitions in part satisfy their identification as plains but also exhibit characteristics that may not be typical of plans, and this may lead to an inaccurate classification. The boundary represents the part

of the plain where the geomorphological semantics and labels change. The fundamental characteristics of plains, i.e. flat terrain, are defined as the plain core and quantified by slope angle in the previous step. The other elements are determined based on the cores. For example, areas outside the plain core that have a relatively low relief should also be considered plains in the geomorphological sense, although segmentation based on slope characteristics may fail to identify them as such due to emphasis being placed on local changes in topography (Figure 2g). These introduces patches in the extraction of plains that may fragment the integrity of larger plains. Furthermore, the resulting landscape segments may themselves contain fragments that reflect local topographic changes but do not represent actual landform objects as recognized geomorphologically. It is challenging to correct all such fragments across complex terrain scenarios at the global scale, thus limiting the feasibility of automated global landform classification.

To address these issues, as the second step in our classification process, we introduce the concept of accumulated cost (AS) and develop an AS derivative that quantifies the attributes of plain transitions by calculating the AS along a path that has the lowest slope cost (Figure 2b). In this process, the core is the typical extracted in the previous step, and the cost surface is the slope gradient. The AS is calculated as the minimum cumulative cost of each position to the nearest plain core along a specific path. In the AS calculation of general position, this algorithm employs an iteration starting from the cell closest to the cores and follows the calculation principle shown in Figure 2c to compute the minimum accumulated slope of each cell to the core. The completed area is then expanded until all grids are associated with increasing costs. This process follows the geospatial analysis principle of the minimum accumulated cost (Sechu et al., 2021). The tool of distance accumulation in ArcGIS Pro can achieve this calculation. Segmenting landforms through the determination of the thresholds for landform derivatives is one of the most common methods used in geomorphological studies and transforms geomorphological qualitative perception towards quantitative computation. As shown in Figure 2d, due to differences in topographic characteristics between plains and mountains, the AS has a low rate of increase in the areas classified as plains and a high rate of increase in rugged areas. This phenomenon reduces the difficulty of determining an appropriate AS threshold, which can be achieved by searching for abrupt changes in the AS profile. In this step, taking into consideration the geomorphological perspective, the threshold of AS (T_2) is recommended to be 1500-2000 based on the pre-experimental results conducted on numerous samples worldwide. This threshold range is provided as a reference but gentle adjustments to the thresholds may be required in some special areas, such as small islands, through human-computer interaction. In some cases, such as small islands where traditional watershed and TIN-based methods tend to struggle, it may exceed the recommended threshold range. Areas where the AS value is less than T_2 are regarded as plains, and the remaining areas are mountains. Through the above segmentation, we can obtain the boundary of plain and construct the complete plain area consisting of core, variant and boundary. As shown in Figures 2g and h, this novel workflow exaggerates the difference between the plains and mountains and converts the local slope into an indicator of global landform characteristics. This novel method avoids the negative effect of local window analysis and is beneficial for maintaining the landform semantics for each block.

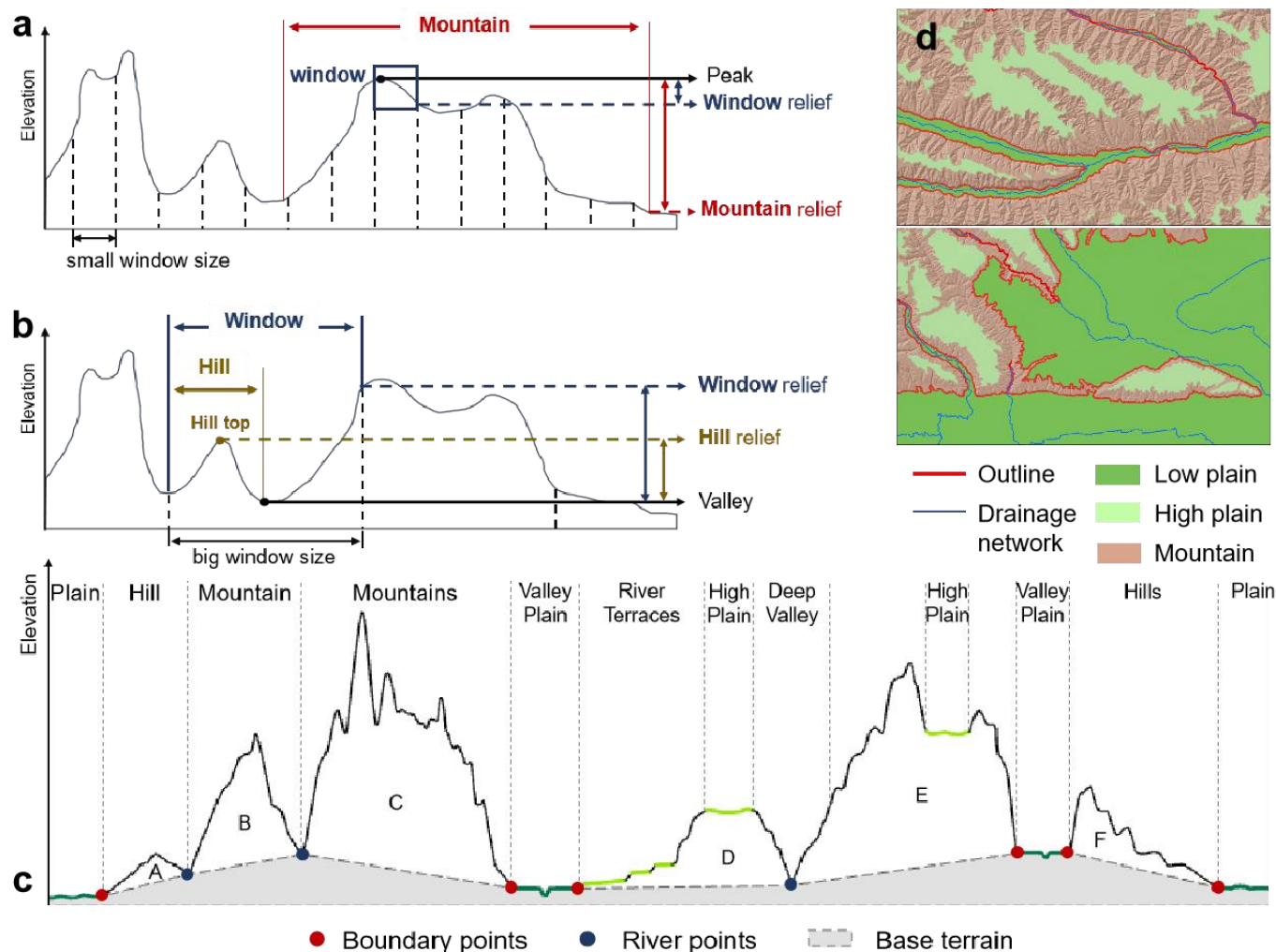


Figure 3. Uncertainty in relief calculation based on the window analysis. a and b the relationship between different windows and topographical relief. c schematic diagram illustrating the base terrain of mountains. d features used to create TIN and build base terrain.

In this step, we focus on the differences of terrain relief to achieve the comprehensive classification of L2 landforms. Terrain relief refers to the difference in elevation between the highest and lowest points within a particular spatial unit. This factor significantly influences landform classification. However, commonly employed indices reflecting topographic relief are achieved using a window of fixed size such as 3×3 , 5×5 pixels, or larger (Maxwell and Shobe, 2022), a method that fails to account for geomorphological semantics, and which therefore disregards the integrity of a mountain. Window size has a significant impact on results of relief calculation. As shown in Figures 3a and b, window analysis tends to disrupt the integrity and continuity of geomorphological elements. Moreover, a small window size is insufficient to capture the entire mountain, particularly in the case of large mountains, while a large window size may incorporate other mountains and fail effectively to capture the relief. The uncertainty introduced by window size further increases the difficulty of global classification and mapping based on relief. Even the multi-scale synthesis approaches can effectively mitigate scale-dependent limitations, these methods still inherently face challenges associated with determining appropriate scales ranges in algorithms.

Therefore, we propose a new method for relief quantification method which do not rely on the traditional window-based

calculation. In this paper, the surface relief index (SRI) is defined as the degree of relative relief to the flat areas surrounding the mountain. We regard the elevation at the foot of the mountain as the base elevation and then calculate the elevation difference between each position on the mountains and the base elevation. Compared to the traditional method of relief calculation (e.g., difference in elevation within a particular window size), SRI considers the vertical elevation differences between the surface and the mountain base, which is more suitable for the objectives in landform-related studies such as mountainous climate and biodiversity.

This step includes three sub-procedures. Firstly, we constructed the mountain extent as the foundation for subsequent calculation. The plain boundary lies at the foot of landforms classified as mountain, which is suitable to represent the extent of mountains. However, when the area of the mountain is large, and the base elevation is constructed only on the basis of the plain boundary, the result cannot reflect the real terrain relief. To refine the representation of surface relief, we introduce linear features representing the rivers. These additional lines can be obtained through DEM based hydro-analysis (Li et al., 2021). In order to ensure that plains at high elevations do not interfere with the definition of the mountain unit, since these are, in effect, part of the mountain range (Figure 3c). We exclude high elevation plains (marked in light green in Figure 3d) that have no fluvial features to retain the integrity of the associated mountain range. Figure 3d shows the final elements involved in establishing the base elevation, which corresponds to the boundary of the low altitude plains and fluvial features (marked in red in Figure 3d). Secondly, we constructed the base elevation to support the calculation of the SRI. In this case, the mountain extent, which replaces the analysis window in traditional relief calculation, is used to construct the base elevation. Specially, we constructed the triangulated irregular network (TIN) based on the position extracted in the first step and then regard the elevation value in TIN as the base elevation. The construction of TIN can be achieved in ArcGIS Pro through create TIN. Thirdly, the SRI is obtained by calculating the difference between each cell height and its corresponding base elevation. This novel method provides a more appropriate representation of the underlying terrain.

2.2.4 Type refinement for L3

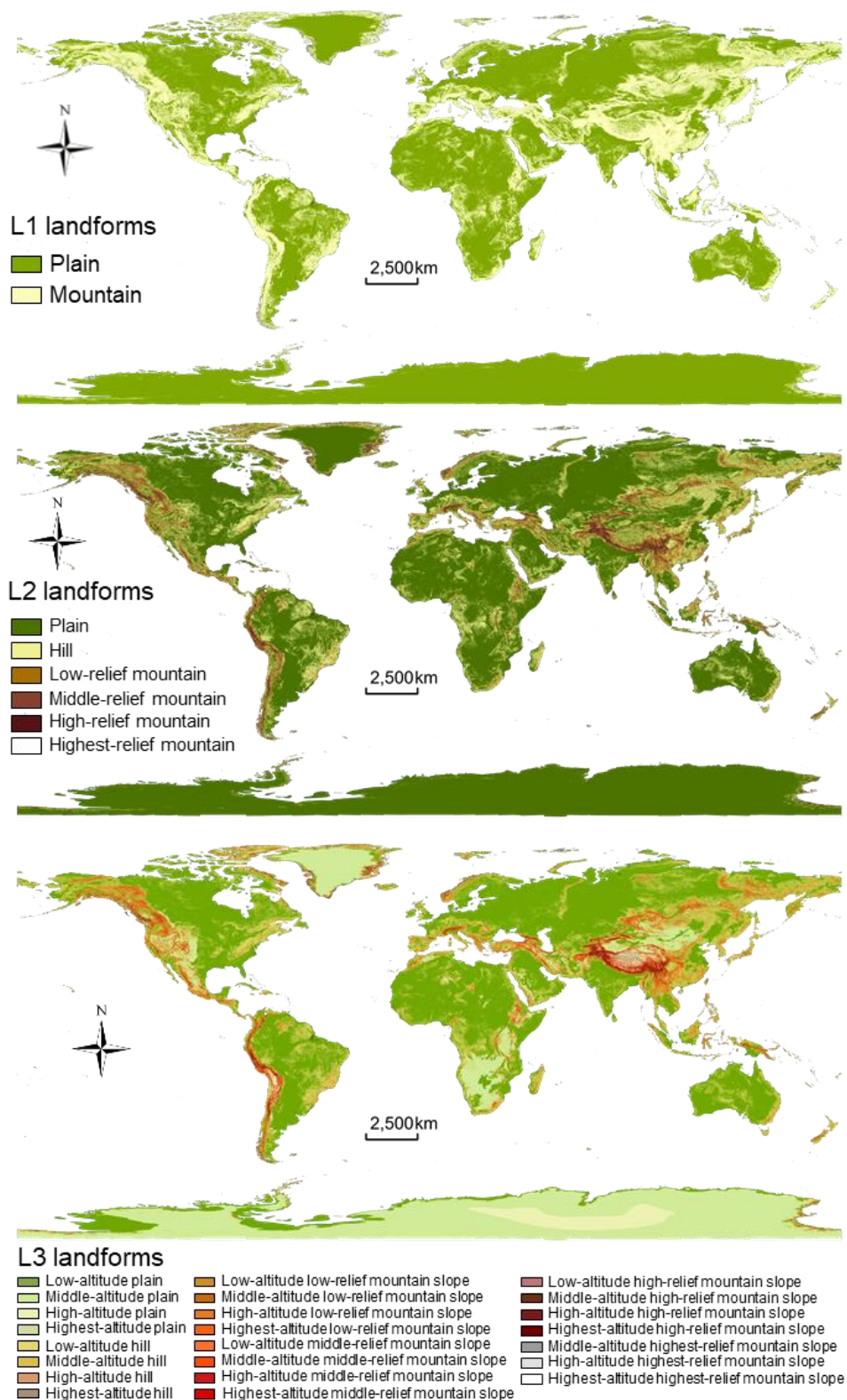
According to the results of previous studies (Zhou et al., 2009), we constructed the classification criteria shown in appendix of Table A1. For the plains, we use altitudes of 1000m, 3500m and 5000m as break points to generate low-, middle-, high- and highest-altitude landforms. Mountains are classified as hill, low-relief, middle-relief, high-relief, and highest-relief mountains, based on threshold SRI values of 200m, 1000m, 3500m and 5000m. In all, this yields 6 classes in L2 and 23 classes in L3.

2.2.5 Post-processing

Following completion of the above processes, a map is generated that includes all the basic landform units. However, due to interference caused by the existence of locally steep changes in topographic relief, this output still contains some features in the plain areas misclassified as hills. Meanwhile, although the data we used are of high resolution and good quality, outliers and/or data noise remain. Such anomalies may result in small landform blocks with relatively low terrain relief and, in accommodating this, we designed an optimization process to correct hill misclassification. We used area and SRI as reflecting their characteristics (e.g. fragmented and relatively low relief). Considering the application of landform data in geomorphologic mapping and the resolution

of basic data, we determined that our study corresponds approximately to the equivalent of 1:200,000 geomorphological mapping. Under the conditions of 1:200,000 scale, the minimum displayable patch size is approximately 0.16 km². The SRI threshold is derived from (Zhou et al., 2009), which defines plains as the blocks with relief of less than 30 metres. Therefore, blocks with areas of less than 0.16 km² and SRIs below 30 metres are regarded as misclassified blocks which are then integrated as part of the surrounding plains.

Meanwhile, we designed an additional step to optimize the results for desert areas. Many arid regions are characterized by dunes, which are distinctive aeolian landforms of varying shape and size constructed from unconsolidated sand (Hugenholtz et al., 2012). Dunes are generally smaller in scale than mountains and this challenges our approach to basic landform mapping (Shumack et al., 2020), increasing the difficulty of accurate dune mapping. In this study, we regarded sand dunes as hills due to their morphological similarity. However, due to the variation of dune size and shape, it is challenging to correctly classify these dunes as hills according to our proposed method. Therefore, we design an optimization step to correct the classification results in which dunes and inter-dune areas are separated and identified according to their altitude and SRI. Firstly, on the basis of on their geomorphological characteristics, remote sensing images, and hillshade maps, we demarcated the major global sand desert regions. Secondly, we used the DEM to extract the topographic feature lines by surface analysis of extracting desert feature lines. Employing the SUI calculation as for other regions, we then constructed the base terrain, in this case, the river networks were extracted with the threshold T_{D1} of 20000, and then we extracted sampling points from these networks to construct TINs. We calculated the SRI and then set the segmented threshold T_{D2} . Due to inconsistencies in the scale of dunes worldwide, we applied an adjustable T_{D2} ranging from 2m to 10m. Areas less than T_{D2} are defined as inter-dunes (equivalent to plains in the basic landform classification). All patches smaller than T_{D3} 0.02km² were regarded as fragments and integrated into the surrounding vector blocks. Finally, we employed the smoothing tool to ensure appropriateness of the landform boundary.



272
273 **Figure 4. Results of the basic global landform classification with 30 m resolution.** a, b and c represent the L1, L2 and L3
274 landforms, respectively.

275 Figure 4 shows the global landform classification results based on the abovementioned framework. This hierarchical dataset
276 provides a more comprehensive understanding of the Earth surface. To visualize the results in detail, three typical regions are

selected to demonstrate the performance of the GBLU dataset. Figure 5 shows the GBLU in typical regions and corresponding remote sensing image from Esri world imagery. The selected regions contain examples of the main landforms on Earth, as well as transition areas of different landforms. In the mountainous areas as shown in Figure 5a, mountain range and valley orientation are clearly discernible, which together form the fundamental structure for expressing mountain. The GBLU clearly illustrates the transition zones between mountains and plains, as well as potential floodplains. While such phenomena are visually discernible in remote sensing imagery, using our proposed framework, they are extracted based on quantified morphological characteristics. The abundant information on the landform composition provided by GBLU can facilitate study of areas with high geomorphological value, such as fjords (Figure 5b). In desert areas Figure 5c, GBLU effectively illustrates the transitional patterns between dunes and depressions. Based on abundant morphological characteristics, GBLU can depict sand dune boundaries that are strikingly consistent with those visible in imagery. This further underscoring the performance of GBLU in capturing detailed geomorphic features across varied terrains.

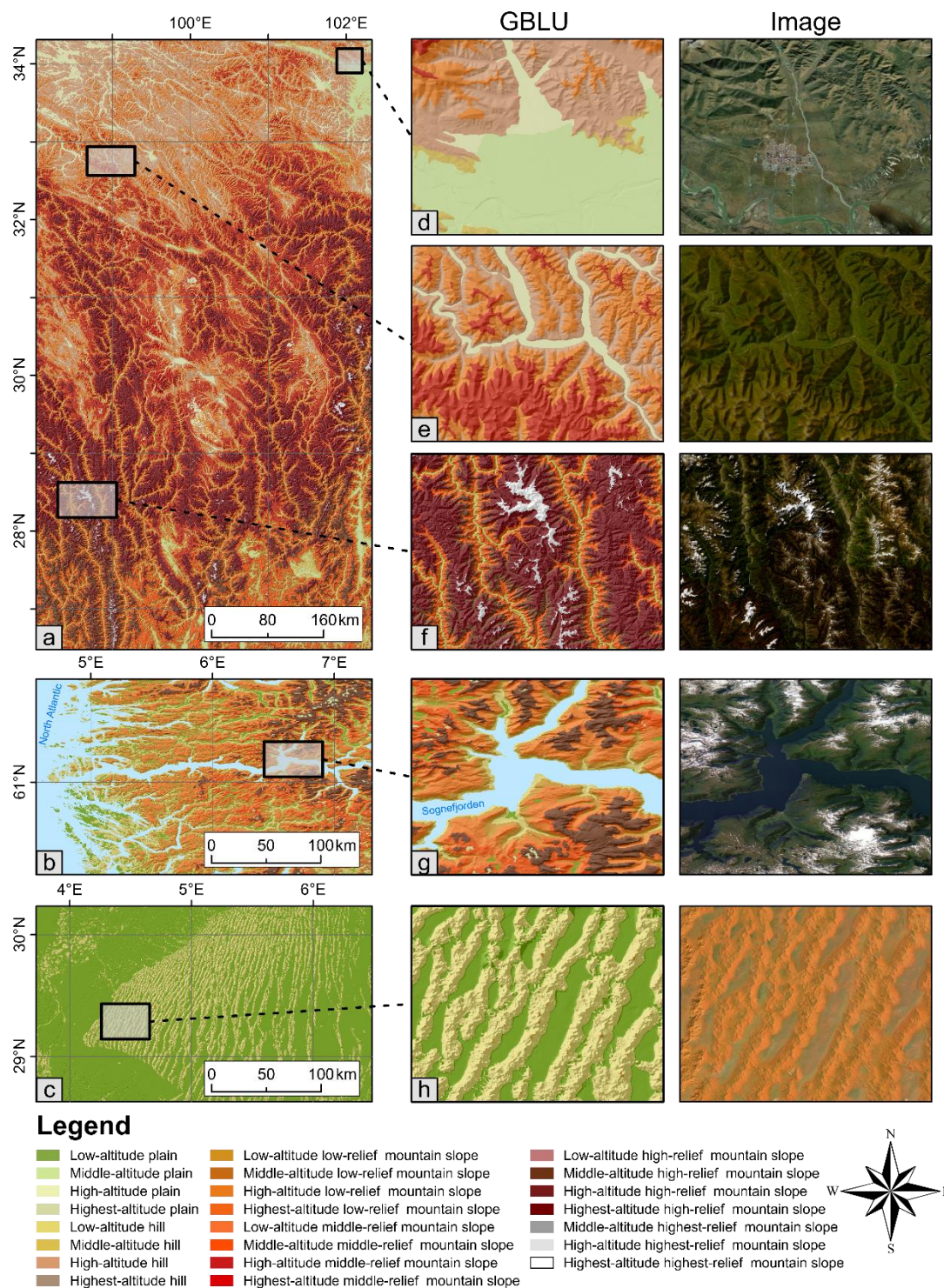
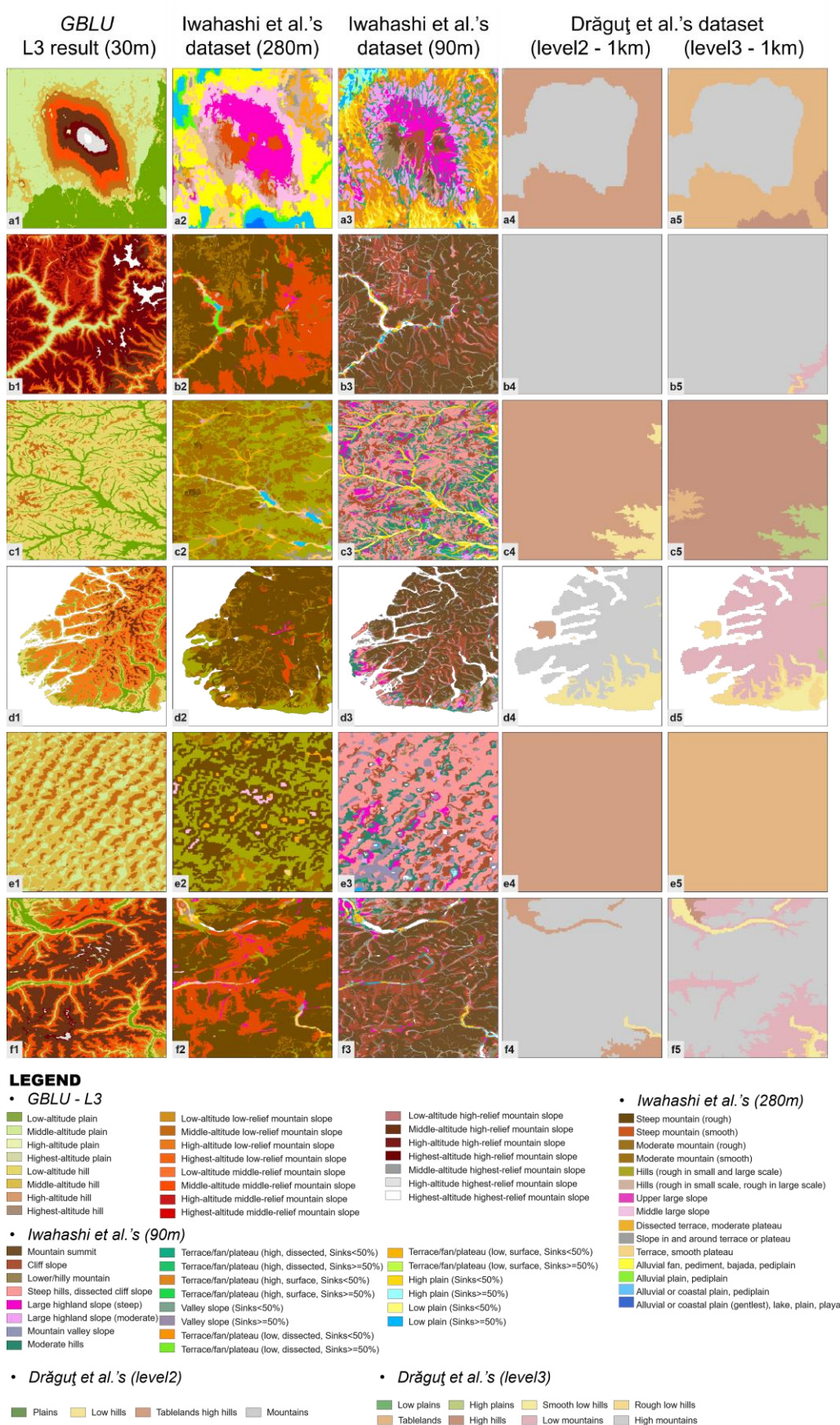
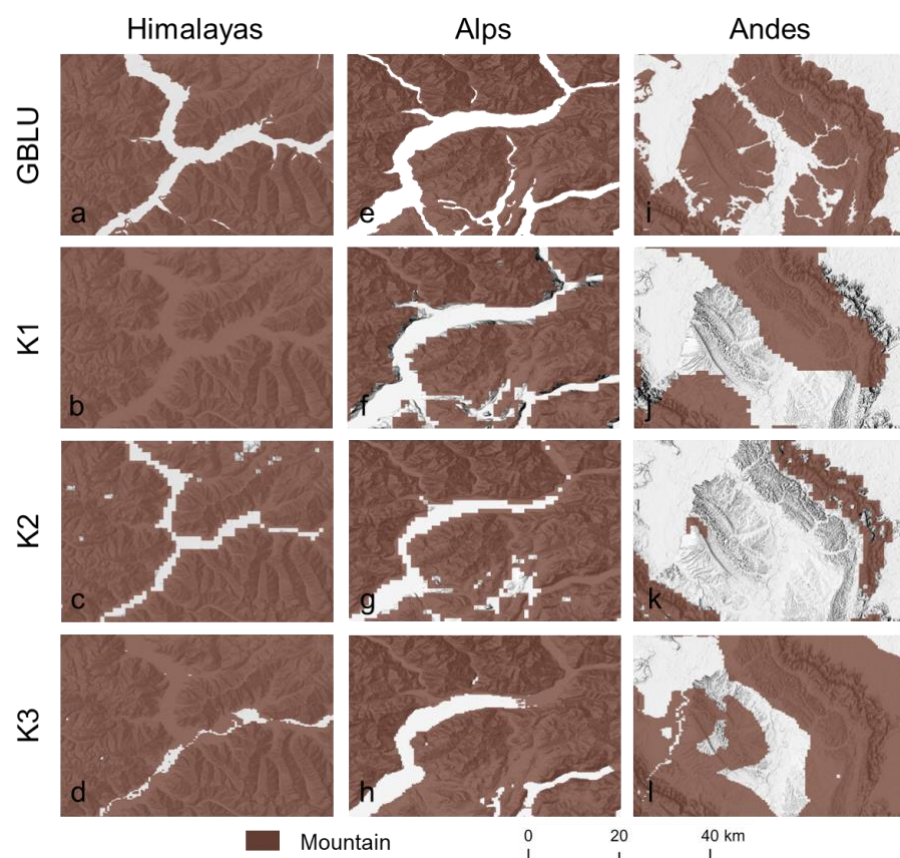


Figure 5. Comparison of landform classification results and remote sensing imagery. a eastern part of the Tibetan Plateau. b the Fjord coast in western Norway. c desert area in the central Sahara. e-h are local enlarged areas.



293 **Figure 6. Comparison of GBLU with other landform classification results.** Selected study areas, from top to bottom, are as
294 follows: a. the Kilimanjaro, b. Namcha Barwa in Himalaya, c. Greater Khingan Mountains, d. Fjords in New Zealand, e. Badain
295 Jaran Desert and f. Central Alps.

296 We conducted comparisons between the GBLU dataset and multiple other datasets to comprehensively evaluate our
 297 results. Specifically, we compared the outcomes of five landform classifications across a range of sample areas. The most
 298 significant improvement achieved by applying GBLU is the increased detail in representing terrain features. The GBLU-based
 299 landform classification markedly enhances delineation of independent landforms, such as dunes and mountains, which have
 300 clear boundaries and serve as key elements in the analysis of spatial structure and interactions. Meanwhile, the valley-like
 301 objects can also be reflected by GBLU. The classification systems of Drăguț and Blaschke (2006) are similar to GBLU but
 302 have a coarser resolution of 1 km, making them less effective in capturing terrain details. Figure 6 illustrates that there is a
 303 variation in the understanding of landform types among different scholars. As mentioned before, Iwahashi's results align more
 304 closely with terrain classification systems. They represent a lot of slope details such as flow channel on the volcanic slopes.
 305 In this paper, we consider landforms of plain or mountain to represent larger scales relative to terrain objects like "slope."
 306 Therefore, in designing the classification system, we think that categorizing 'slope' at the same level as 'plain' or 'mountain'
 307 can lead to some comprehension difficulties. Therefore, GBLU offers a more comprehensive landform classification system
 308 and expresses the integrity of landform objects more closely aligned with the ontological understanding of landforms.



309
 310 **Figure 7.** Comparison between the GBLU and three mountain definitions presented on the Global Mountain Explorer
 311 (<https://rmgsc.cr.usgs.gov/gme/>)

312 We conducted a more detailed comparison for mountain regions to reference from the Global Mountain Explorer as reference
 313 data. The GMBA dataset contains three subsets using the DEM with spatial resolutions of 1000 m, 1000 m and 250 m to generate
 314 global mountain maps. These three datasets (e.g., K1, K2 and K3) are produced by analyzing the morphological derivatives, using

a moving neighbourhood analysis window for relief, elevation, and slope (Kapos et al., 2000; Karagulle et al., 2017; Körner et al., 2011). That similar indicators are used in the associated classification and mapping processes indicates the comparability of the GMBA and the GBLU datasets, although due to differences in the category settings among the GBLU and the GMBA datasets, the comparison in this study focused only mountains. As shown in Figure 7, the GBLU dataset clearly outperforms the other three datasets in depicting mountain details, especially in representing valleys. This can be seen in Figures 7a-h, whereby the K1,K2 and K3 data exhibits separated upland blocks in mountainous regions with complex and intense terrain variations, and fails to represent continuous valleys.

Due to differences in classification systems and indices, it is challenging to conduct further quantitative comparisons between GBLU and other results. To facilitate comparison between these datasets, we merged some classes in the datasets to maintain classification consistency. For example, we merged mountain summit and cliff slope sections into ‘mountain’ as per merging criteria described in Table A2. Overall, GBLU results are consistent with other systems in terms of the macroscopic landform patterns. The merged results indicate that Iwahashi and Yamazaki's dataset performs better in representing plains boundaries and their shapes.

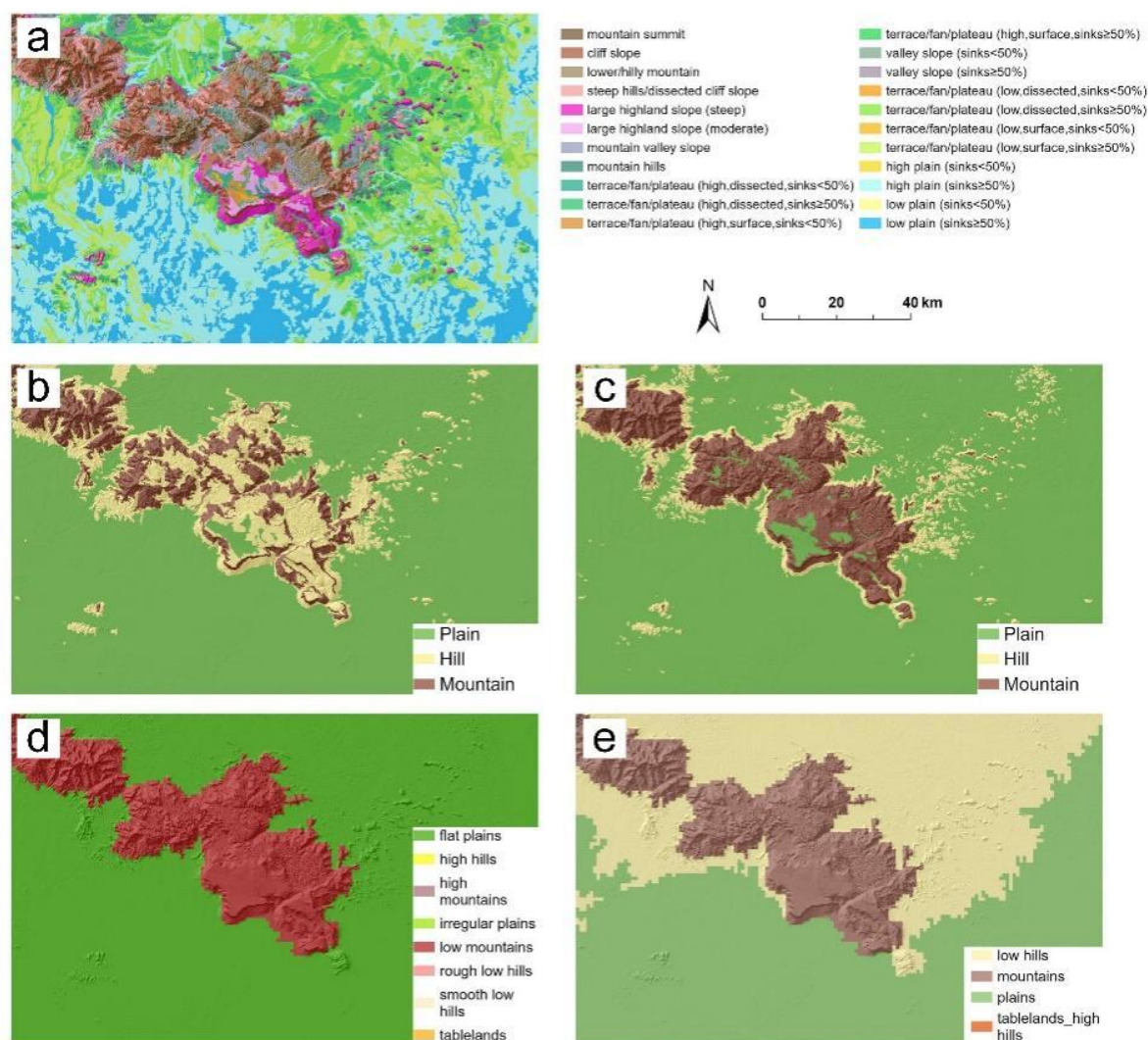
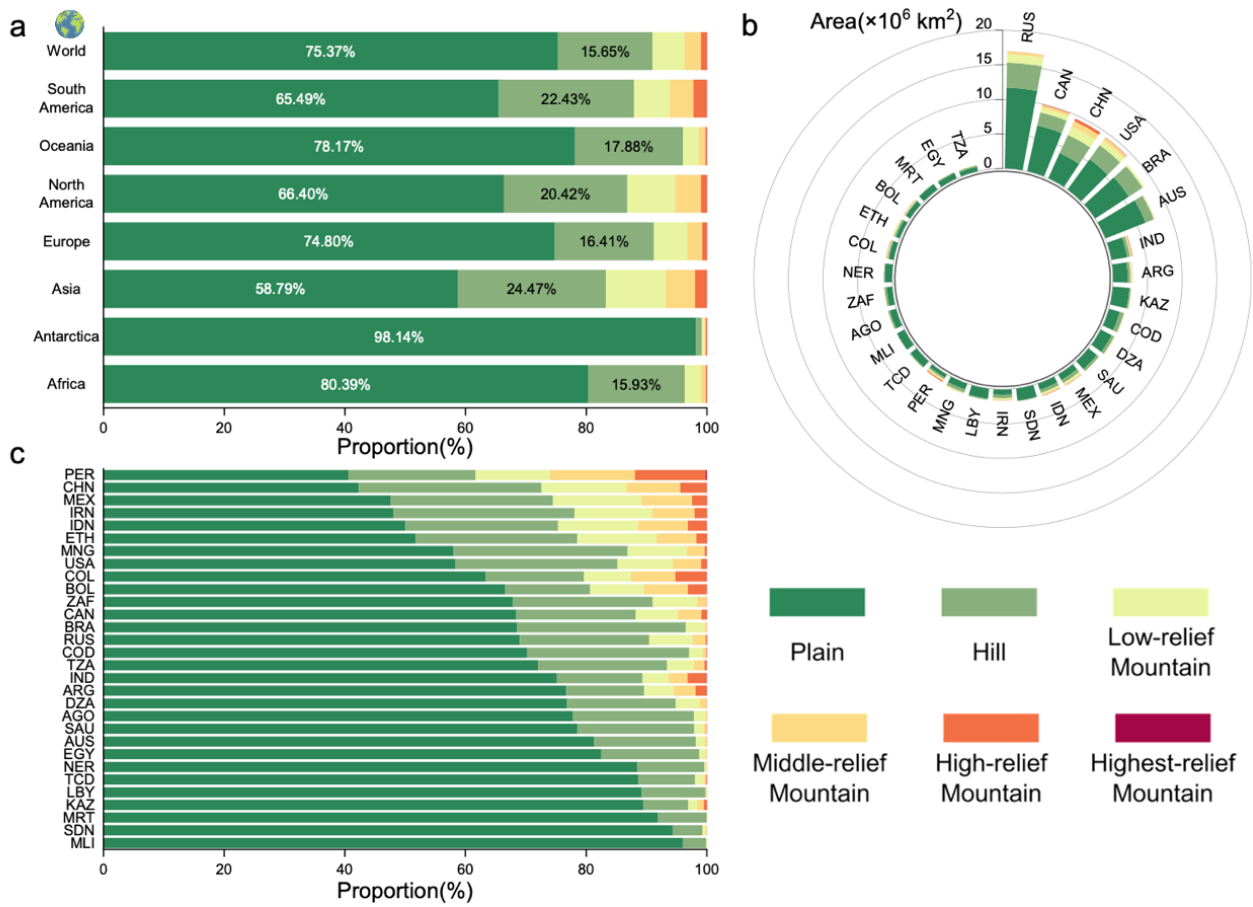


Figure 8. Classification result of the GBLU for an existing landform mapping dataset in the Amazon River basin.

a Iwahashi and Yamazaki (2022) original result; **b** adjusted Iwahashi and Yamazaki ,2022 result through merging landform

330 classes; **c** GBLU result; **d** Drăguț and Eisank (2012) result (level 3); **e** Drăguț and Eisank, 2012 result (level 2).

331 **3.4 Global landform composition**



332
333 **Figure 9. Area and proportional area statistics at continental and national scales.** **a** Proportion of primary landforms on each
334 continent. **b** Area of primary landform types in the top 30 countries ranked by area. **c** Proportion of primary landform types in the
335 top 30 countries ranked by area. Full names of countries listed can be found in Table A3.

336 We have used a cell size of 500 m x 500 m to accurately assess the proportions of primary landforms across continents
337 worldwide, thereby yielding insights into their spatial variations. The findings indicate that approximately 75% of the global land
338 area comprises plains, while some 16% consists of hills, with the remaining portion classified as mountains (Figure 9a). In terms of
339 the distribution of landform composition, Asia exhibits a very distinctive pattern, since plains cover only 59% of its land area, the
340 lowest among all continents, while there is a significantly higher proportion of hills and mountains, consistent with its pronounced
341 topographic diversity. Compared to the global average, the presence of continental marginal mountain chains results in a
342 significantly lower proportion of plains, and correspondingly higher proportion of mountains, in both North and South America.
343 Indeed, South America has very substantial areas of high relief mountains, while Africa is distinguished by the dominance of
344 extensive plains.

345 We further conducted a comprehensive analysis of landform types and their proportions at the national and regional scale
346 across all countries and regions worldwide to reveal patterns of variation. Figure 9b illustrates the proportion of primary landform

types in the top 30 countries ranked by area, while Figure 9c depicts the standardized proportion of the landform types within these countries, sorted based on the proportion of plains. China's diverse and rugged topography is evident in its significantly high proportion of mountains, while Peru contains the lowest proportion of plains, as mountainous terrain there occupies over 60% of its land area.

3.4 Dataset usage note

In this section, we highlight the results of experiments performed to analyse the relationship between landforms, climate and land cover to highlight the potential applications of GBLU. Based on the high resolution landform classes provided by GBLU, we can explore the complex and in-depth relationships between landforms, climate, and land cover. The climate data is the widely used 1-km Köppen-Geiger climate classification maps in 1991–2020 (Beck et al., 2023) and the land cover data is from FROM-GLC 30m in 2017 (Yu et al., 2013).

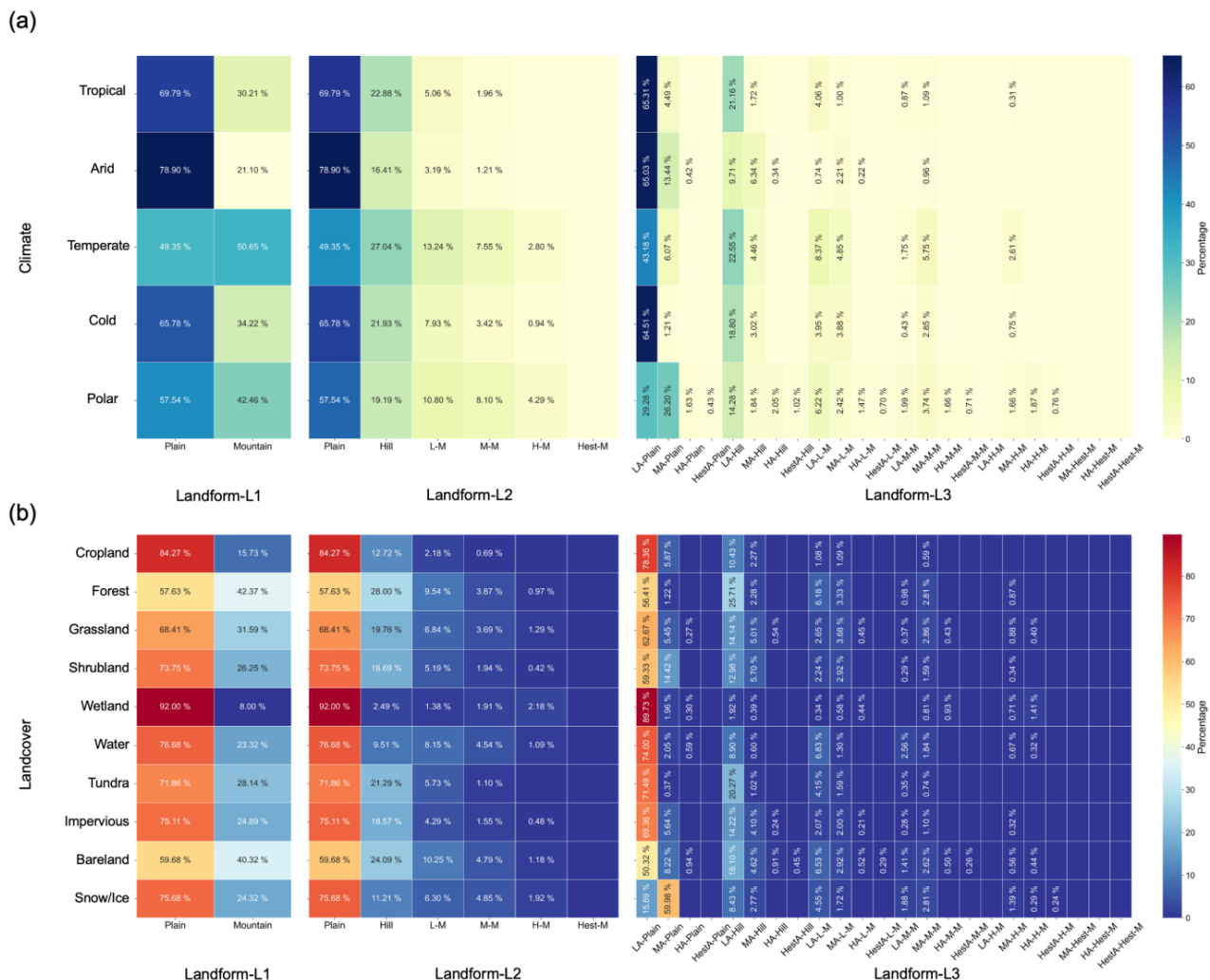


Figure 10. Relationship of landform types to climate and land cover. (a) and (b) show the proportions of the three classes of landform types in different climatic and land cover regions respectively. Values less than 0.2% are not labeled with numbers.

The enhanced resolution and detail of the GBLU enables subtle variations in the Earth's surface to be captured, which is highly valuable in understanding interactions between geomorphology and other factors. As shown in Figure 10, landform distribution in

temperate zones suggests a unique blend of climatic conditions and geomorphologic processes, fostering a diverse array of landforms. In the climatic zones of tropical, arid, and cold regions, we observe that low-altitude plains and hills are most prominent. For polar areas, a larger proportion of the area is located at higher altitudes than in other climate zones. Regarding land cover analysis (excluding the South Polar area), cropland occupies 84.27% of plains and 15.73% of mountains, yielding useful insights for analyzing cultivated land productivity. Meanwhile, forests and bare land are more prevalent in mountains, more especially in hills. Additionally, the percentage of many ecologically significant biomes, such as forests, grasslands, wetlands, tundra, and water bodies, in plains and mountainous regions has been brought up to date. This is potentially valuable for assessing the quality of ecological environments and carbon stocks.

The GBLU provided in this work has obvious applications in geomorphology but also in other fields and can, moreover, play a fundamental role in supporting the identification of landforms that incorporates domain background. For example, identification of a landscape element as ‘tableland’ is complex, differs between disciplines, and requires that both morphological and evolutionary characteristics be accounted for. The GBLU can be integrated with additional observations to map the occurrence and distribution of tablelands through the delineation of segments that are elevated, flat, and surrounded by steep escarpments. There is also significant potential for the application of GBLU to other fields (such as geology, hydrology and ecology) focusing on the natural environment. For example, for ecologists, biodiversity distribution across different landform regions is one of the most significant issues and central to understanding the nature of ecosystem change. At the regional scale, contrasting geomorphological conditions are known to promote isolation of biological populations, influencing community structure and function, as well as evolution. Meanwhile, the interaction between geomorphology and biogeography may result in complex biogeomorphological dynamics. The feedback between physical, ecological and evolutionary components constituting biogeomorphological systems is an important element of the evolution of the Earth’s surface.

4. Dataset access

Global Basic Landform Units (GBLU v1.0) is stored in the Deep-time Digital Earth Geomorphology platform and Zenodo (Yang et al., 2024; <https://doi.org/10.5281/zenodo.13187969>). The data are stored in Esri shapefile format using the coordinate system WGS84. Total size of the dataset is 150GB, with 6,849,306 independent landform blocks. In order to facilitate application, we employed a $1^{\circ} \times 1^{\circ}$ grid to tile the data for storage, with 25,252 file tiles in all. We distinguish the types of landform units by coding attributes of the elements. Additionally, we provide a rasterized dataset (at 30m resolution) using the coordinate system of WGS84. Values of the cells represent the codes of L3 types. In the attribute table, field “code0” is the landform type code of the first level, field “code1” is the landform type code of the second level and field “code2” is the landform type code of the L3.

5. Conclusion

This study provides a novel global landform classification dataset (GBLU) with a resolution of 1 arc-second (approximately 30 m). In this study, we propose a novel framework for global landform mapping to significantly improve

the quantitative evaluation of geomorphological features. The key output is the release of the GBLU dataset that is suited to applications across multiple disciplines, including geography, geology, ecology, and hydrology. Global-scale analysis of attributes within the GBLU reveals the composition and distribution of global landforms that enables comparison between regions and continents. The results emphasize the notable heterogeneity of Asia in general, and of China in particular, in terms of geomorphological diversity. The GBLU outperforms previous datasets in expressing landform details, providing an opportunity to investigate the Earth's natural resources. The resolution of the GBLU is similar to that of the current mainstream remote sensing data, which makes combined use of the data relatively simple. We believe that this dataset can provide abundant and detailed geomorphological information for the field of earth sciences, facilitating further advancements in related research.

Appendix A

Table A1. Classification of global basic landform types





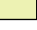

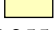
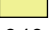
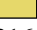






















L1	Code	Colors (RGB)	L2	Code	Colors (RGB)	L3	Code	Colors (RGB)
Plain	1	 129,168,0	Plain	11	 76,115,0	Low-altitude plain	111	 112,168,0
						Middle-altitude plain	112	 209,235,152
						High-altitude plain	113	 237,242,179
						Highest-altitude plain	114	 213,217,164
Mountain	2	 255,255,190	Hill	21	 240,242,148	Low-altitude hill	211	 230,216,106
						Middle-altitude hill	212	 220,191,75
						High-altitude hill	213	 217,155,110
						Highest-altitude hill	214	 170,141,117
			Low-relief Mountain	22	 168,112,0	Low-altitude low-relief mountain slope	221	 209,145,28
						Middle-altitude low-relief mountain slope	222	 198,106,20
						High-altitude low-relief mountain slope	223	 237,122,24
						Highest-altitude low-relief mountain slope	224	 244,100,18
			Middle-relief Mountain	23	 137,65,47	Low-altitude middle-relief mountain slope	231	 253,120,25
						Middle-altitude middle-relief mountain slope	232	 255,76,0
						High-altitude middle-relief mountain slope	233	 201,30,9
						Highest-altitude middle-relief mountain slope	234	 220,0,0
			High-relief Mountain	24	 86,20,24	Low-altitude high-relief mountain slope	241	 193,119,120
						Middle-altitude high-relief mountain slope	242	 110,50,20
						High-altitude high-relief mountain slope	243	 114,4,9
						Highest-altitude high-relief mountain slope	244	 115,0,0
			Highest-relief Mountain	25	 255,255,255	Middle-altitude highest-relief mountain slope	252	 156,156,156
						High-altitude highest-relief mountain slope	253	 225,225,225
						Highest-altitude highest-relief mountain slope	254	 255,255,255

Table A2. Merging the GBLU results to enable comparison with the results of Iwahashi and Yamazaki.

	Terrain22	Gcluster15	Sinks	legend
Mountain	1	2	1,0	Mountain summit
	2	3	1,0	Cliff slope
	3	13	1,0	Lower/hilly mountain
	4	12	1,0	Steep hills/dissected cliff slope
	5	5	1,0	Large highland slope (steep)
	6	4	1,0	Large highland slope (moderate)
	7	14	1,0	Mountain valley slope
	8	10	1,0	Moderate hills
Hill	9*	11	0	Terrace/fan/plateau (high, dissected, Sinks < 50%)
	10	11	1	Terrace/fan/plateau (high, dissected, Sinks ≥ 50%)
	11	7	0	Terrace/fan/plateau (high, surface, Sinks < 50%)
	12	7	1	Terrace/fan/plateau (high, surface, Sinks ≥ 50%)
	13*	8	0	Valley slope (Sinks < 50%)
	14	8	1	Valley slope (Sinks ≥ 50%)
Plain	15*	9	0	Terrace/fan/plateau (low, dissected, Sinks < 50%)
	16	9	1	Terrace/fan/plateau (low, dissected, Sinks ≥ 50%)
	17*	6	0	Terrace/fan/plateau (low, surface, Sinks < 50%)
	18	6	1	Terrace/fan/plateau (low, surface, Sinks ≥ 50%)
	19*	1	0	High plain (Sinks < 50%)
	20	1	1	High plain (Sinks ≥ 50%)
	21*	15	0	Low plain (Sinks < 50%)
	22	15	1	Low plain (Sinks ≥ 50%)

Table A3. Countries' names and their abbreviations.

NAME	Abbreviations
Russian Federation	RUS
Canada	CAN
Peoples Republic of China	CHN
United States of America	USA
Federative Republic of Brazil	BRA
Commonwealth of Australia	AUS
Republic of India	IND
Argentina	ARG
Republic of Kazakhstan	KAZ
Democratic Republic of Congo	COD
Democratic People	DZA
Kingdom of Saudi Arabia	SAU
United States of Mexico	MEX
Republic of Indonesia	IDN
Republic of the Sudan	SDN
Islamic Republic of Iran	IRN
Great Socialist People	LBY
Mongolia	MNG
Republic of Peru	PER
Republic of Chad	TCD
Republic of Mali	MLI
Angola	AGO
Republic of South Africa	ZAF
Republic of Niger	NER
Republic of Colombia	COL
Federal Democratic Republic of Ethiopia	ETH
Republic of Bolivia	BOL
Islamic Republic of Mauritania	MRT
Arab Republic of Egypt	EGY
United Republic of Tanzania	TZA

Author contribution

Xin Yang, Guoan Tang and Michael Meadows designed the study.

Xin Yang, Sijin Li, Junfei Ma, Yang Chen and Xingyu Zhou performed the analysis.

Xin Yang and Sijin Li wrote the first version of the manuscript.

Fayuan Li, Liyang Xiong and Chenghu Zhou coordinated the work and reviewed the manuscript.

Sijin Li, Junfei Ma, Yang Chen and Xingyu Zhou assisted with quality control and reviewed the manuscript.

All the authors contributed to the final version of the manuscript.

Competing interests

The authors declare that they have no conflict of interest.

References

- Amatulli, G., Domisch, S., Tuanmu, M.-N., Parmentier, B., Ranipeta, A., Malczyk, J., and Jetz, W.: A suite of global, cross-scale topographic variables for environmental and biodiversity modeling, *Sci Data*, 5, 180040, <https://doi.org/10.1038/sdata.2018.40>, 2018.
- Amatulli, G., McInerney, D., Sethi, T., Strobl, P., and Domisch, S.: Geomorpho90m, empirical evaluation and accuracy assessment of global high-resolution geomorphometric layers, *Sci Data*, 7, 162, <https://doi.org/10.1038/s41597-020-0479-6>, 2020.
- Beck, H. E., McVicar, T. R., Vergopolan, N., Berg, A., Lutsko, N. J., Dufour, A., Zeng, Z., Jiang, X., van Dijk, A. I., and Miralles, D. G.: High-resolution (1 km) Köppen-Geiger maps for 1901–2099 based on constrained CMIP6 projections, *Scientific data*, 10, 724, <https://doi.org/10.1038/s41597-023-02549-6>, 2023.
- Drăguț, L. and Blaschke, T.: Automated classification of landform elements using object-based image analysis, *Geomorphology*, 81, 330–344, <https://doi.org/10.1016/j.geomorph.2006.04.013>, 2006.
- Drăguț, L. and Eisank, C.: Object representations at multiple scales from digital elevation models, *Geomorphology*, 129, 183–189, <https://doi.org/10.1016/j.geomorph.2011.03.003>, 2011.
- Drăguț, L. and Eisank, C.: Automated object-based classification of topography from SRTM data, *Geomorphology*, 141–142, 21–33, <https://doi.org/10.1016/j.geomorph.2011.12.001>, 2012.
- Dramis, F.: Geomorphological mapping for a sustainable development, *Journal of Maps*, 1, 53–55, <https://doi.org/10.4113/jom.2009.1084>, 2009.
- Dyba, K. and Jasiewicz, J.: Toward geomorphometry of plains-Country-level unsupervised classification of low-relief areas (Poland), *Geomorphology*, 413, 108373, <https://doi.org/10.1016/j.geomorph.2022.108373>, 2022.
- Evans, I. S.: Geomorphometry and landform mapping: What is a landform?, *Geomorphology*, 137, 94–106, <https://doi.org/10.1016/j.geomorph.2010.09.029>, 2012.
- Florinsky, I. V.: An illustrated introduction to general geomorphometry, *Progress in Physical Geography: Earth and Environment*, 41, 723–752, <https://doi.org/10.1177/0309133317733667>, 2017.
- Gallant, A. L., Brown, D. D., and Hoffer, R. M.: Automated mapping of Hammond’s landforms, *IEEE geoscience and remote sensing letters*, 2, 384–388, <https://doi.org/10.1109/LGRS.2005.848529>, 2005.
- Hammond, E. H.: Small-Scale Continental Landform Maps, *Annals of the Association of American Geographers*, 44, 33–42, <https://doi.org/10.1080/00045605409352120>, 1954.
- Hawker, L., Uhe, P., Paulo, L., Sosa, J., Savage, J., Sampson, C., and Neal, J.: A 30 m global map of elevation with forests and buildings removed, *Environ. Res. Lett.*, 17, 024016, <https://doi.org/10.1088/1748-9326/ac4d4f>, 2022.
- Hugenholtz, C. H., Levin, N., Barchyn, T. E., and Baddock, M. C.: Remote sensing and spatial analysis of aeolian sand dunes: A review and outlook, *Earth-Science Reviews*, 111, 319–334, <https://doi.org/10.1016/j.earscirev.2011.11.006>, 2012.
- Iwahashi, J. and Pike, R. J.: Automated classifications of topography from DEMs by an unsupervised nested-means algorithm and a three-part geometric signature, *Geomorphology*, 86, 409–440, 2007.

Iwahashi, J. and Yamazaki, D.: Global polygons for terrain classification divided into uniform slopes and basins, *Prog Earth Planet Sci*, 9, 33, <https://doi.org/10.1186/s40645-022-00487-2>, 2022.

Iwahashi, J., Kamiya, I., Matsuoka, M., and Yamazaki, D.: Global terrain classification using 280 m DEMs: segmentation, clustering, and reclassification, *Prog Earth Planet Sci*, 5, 1, <https://doi.org/10.1186/s40645-017-0157-2>, 2018.

Jasiewicz, J. and Stepinski, T. F.: Geomorphons — a pattern recognition approach to classification and mapping of landforms, *Geomorphology*, 182, 147–156, <https://doi.org/10.1016/j.geomorph.2012.11.005>, 2013.

Kapos, V., Rhind, J., Edwards, M., Price, M., Ravilious, C., and Butt, N.: Developing a map of the world's mountain forests., *Forests in sustainable mountain development: a state of knowledge report for 2000*, Task Force For. Sustain. Mt. Dev., 4–19, <https://doi.org/10.1079/9780851994468.0004>, 2000.

Karagulle, D., Frye, C., Sayre, R., Breyer, S., Aniello, P., Vaughan, R., and Wright, D.: Modeling global Hammond landform regions from 250-m elevation data, *Transactions in GIS*, 21, 1040–1060, <https://doi.org/10.1111/tgis.12265>, 2017.

Körner, C., Paulsen, J., and Spehn, E. M.: A definition of mountains and their bioclimatic belts for global comparisons of biodiversity data, *Alp Botany*, 121, 73–78, <https://doi.org/10.1007/s00035-011-0094-4>, 2011.

Li, S., Xiong, L., Tang, G., and Strobl, J.: Deep learning-based approach for landform classification from integrated data sources of digital elevation model and imagery, *Geomorphology*, 354, 107045, <https://doi.org/10.1016/j.geomorph.2020.107045>, 2020.

Li, S., Xiong, L., Hu, G., Dang, W., Tang, G., and Strobl, J.: Extracting check dam areas from high-resolution imagery based on the integration of object-based image analysis and deep learning, *Land Degrad Dev*, 32, 2303–2317, <https://doi.org/10.1002/ldr.3908>, 2021.

MacMillan, R. A. and Shary, P. A.: Landforms and landform elements in geomorphometry, *Developments in soil science*, 33, 227–254, [https://doi.org/10.1016/S0166-2481\(08\)00009-3](https://doi.org/10.1016/S0166-2481(08)00009-3), 2009.

Martins, F. M. G., Fernandez, H. M., Isidoro, J. M. G. P., Jordán, A., and Zavala, L.: Classification of landforms in Southern Portugal (Ria Formosa Basin), *Journal of Maps*, 12, 422–430, <https://doi.org/10.1080/17445647.2015.1035346>, 2016.

Maxwell, A. E. and Shobe, C. M.: Land-surface parameters for spatial predictive mapping and modeling, *Earth-Science Reviews*, 226, 103944, <https://doi.org/10.1016/j.earscirev.2022.103944>, 2022.

Pennock, D. J., Zebarth, B. J., and De Jong, E.: Landform classification and soil distribution in hummocky terrain, Saskatchewan, Canada, *Geoderma*, 40, 297–315, [https://doi.org/10.1016/0016-7061\(87\)90040-1](https://doi.org/10.1016/0016-7061(87)90040-1), 1987.

Shumack, S., Hesse, P., and Farebrother, W.: Deep learning for dune pattern mapping with the AW3D30 global surface model, *Earth Surface Processes and Landforms*, 45, 2417–2431, <https://doi.org/10.1002/esp.4888>, 2020.

Smith, B. and Mark, D. M.: Geographical categories: an ontological investigation, *International Journal of Geographical Information Science*, 15, 591–612, <https://doi.org/10.1080/13658810110061199>, 2001.

Smith, B. and Mark, D. M.: Do Mountains Exist? Towards an Ontology of Landforms, *Environ Plann B Plann Des*, 30, 411–427, <https://doi.org/10.1068/b12821>, 2003.

Snethlage, M. A., Geschke, J., Ranipeta, A., Jetz, W., Yoccoz, N. G., Körner, C., Spehn, E. M., Fischer, M., and Urbach, D.: A hierarchical inventory of the world's mountains for global comparative mountain science, *Sci Data*, 9, 149, <https://doi.org/10.1038/s41597-022-01256-y>, 2022.

Tadono, T., Ishida, H., Oda, F., Naito, S., Minakawa, K., and Iwamoto, H.: Precise Global DEM Generation by ALOS PRISM, *ISPRS Annals of the Photogrammetry, Remote Sensing and Spatial Information Sciences*, II–4, 71–76, <https://doi.org/10.5194/isprsannals-ii-4-71-2014>, 2014.

Xiong, L., Li, S., Tang, G., and Strobl, J.: Geomorphometry and terrain analysis: Data, methods, platforms and applications, *Earth-Science Reviews*, 104191, <https://doi.org/10.1016/j.earscirev.2022.104191>, 2022.

Yu, L., Wang, J., and Gong, P.: Improving 30 m global land-cover map FROM-GLC with time series MODIS and auxiliary data sets: a segmentation-based approach, *International Journal of Remote Sensing*, 34, 5851–5867, <https://doi.org/10.1080/01431161.2013.798055>, 2013.

Zhou, C. H., Cheng, W. M., Qian, J. K., Li, B. Y., and Zhang, B. P.: Research on the classification system of digital land geomorphology of 1: 1000000 in China, *Journal of Geo-Information Science*, 11, 707–724, <https://doi.org/10.3724/SP.J.1047.2009.00707>, 2009.